

Barkhausen noise from precessional domain wall motion

Touko Herranen¹ and Lasse Laurson^{2*}

¹*Helsinki Institute of Physics, Department of Applied Physics,
Aalto University, P.O.Box 11100, FI-00076 Aalto, Espoo, Finland. and*

²*Computational Physics Laboratory, Tampere University, P.O. Box 692, FI-33014 Tampere, Finland*

The jerky dynamics of domain walls driven by applied magnetic fields in disordered ferromagnets – the Barkhausen effect – is a paradigmatic example of crackling noise. We study Barkhausen noise in disordered Pt/Co/Pt thin films due to precessional motion of domain walls using full micromagnetic simulations, allowing for a detailed description of the domain wall internal structure. In this regime the domain walls contain topological defects known as Bloch lines which repeatedly nucleate, propagate and annihilate within the domain wall during the Barkhausen jumps. In addition to bursts of domain wall propagation, the in-plane Bloch line dynamics within the domain wall exhibits crackling noise, and constitutes the majority of the overall spin rotation activity.

Understanding the bursty crackling noise response of elastic objects in random media – domain walls (DWs) [1], cracks [2], fluids fronts invading porous media [3], et cetera – to slowly varying external forces is one of the main problems of statistical physics of materials. An important example is given by the magnetic field driven dynamics of DWs in disordered ferromagnets, where they respond to a slowly changing external magnetic field by exhibiting a sequence of discrete jumps with a power-law size distribution [1, 4]. This phenomenon, known as the Barkhausen effect [5], has been studied extensively, and a fairly well-established picture of the possible universality classes of the avalanche dynamics, using the language of critical phenomena, is emerging [1, 4].

Magnetic DWs constitute a unique system exhibiting crackling noise since the driving field may, in addition to pushing the wall forward, excite internal degrees of freedom within the DW [6]. This effect is well-known especially in the nanowire geometry – important for the proposed spintronics devices such as the racetrack memory [7] – where the onset of precession of the DW magnetization above a threshold field leads to an abrupt drop in the DW propagation velocity (the Walker breakdown [8]), and hence to a non-monotonic driving field vs DW velocity relation [9]; these features are well-captured by the so-called $1d$ models [10].

In wider strips or thin films, the excitations of the DW internal magnetization accompanying the velocity drop cannot be described by precession of an individual magnetic moment. Instead, one needs to consider the nucleation, propagation and annihilation of topological defects known as Bloch lines (BLs) within the DW [11–13]. BLs, i.e., transition regions separating different chiralities of the DW, have been studied in the context of bubble materials already in the 1970’s [13]. Their role in the physics of the Barkhausen effect needs to be studied. The typical models of Barkhausen noise, such as elastic interfaces in random media [4, 14], scalar field models [15] or the random field Ising model (RFIM) [16–18], exclude BLs by construction.

Here, we focus on understanding the consequences of

the presence of BLs within DWs on the jerky DW motion through a disordered thin ferromagnetic film. To this end, we study field-driven DW dynamics considering as a test system a 0.5 nm thick Co film within a Pt/Co/Pt multilayer [19] with perpendicular magnetic anisotropy (PMA) by micromagnetic simulations, able to fully capture the DW internal structure. By tuning the strength of quenched disorder, we match the DW velocity vs applied field curve to the experimental one reported in [19]. This leads to a depinning field well above the Walker field of the corresponding disorder-free system. Hence, when applying a driving scheme corresponding to a quasistatic constant imposed DW velocity, the resulting Barkhausen jumps take place within the precessional regime.

We find that in addition to avalanches of DW propagation, also the in-plane BL magnetization dynamics within the DW exhibits crackling noise, and is responsible for the majority of the overall spin rotation activity during the Barkhausen jumps; the latter dynamics is not directly observable in typical experiments (magneto-optical imaging [20], or inductive recording [21]). The DW can locally move backwards, so it does not obey the Middleton non-passing theorem [22]. Functional renormalization group calculations [23] crucially depend on this property, but we find that in line-like DWs BLs do not change the scaling picture of avalanches if one looks at measures related to DW displacement. Remarkably, simple scaling relations applicable to short-range elastic strings in random media remain valid in the much more complex scenario we consider here.

In our micromagnetic simulations of the DW dynamics, the Landau-Lifshitz-Gilbert (LLG) equation, $\partial\mathbf{m}/\partial t = \gamma\mathbf{H}_{\text{eff}} \times \mathbf{m} + \alpha\mathbf{m} \times \partial\mathbf{m}/\partial t$, describing the time-evolution of the magnetization $\mathbf{m} = \mathbf{M}/M_S$, is solved using the MuMax3 software [24]. In the LLG equation, γ is the gyromagnetic ratio, α the Gilbert damping parameter, and \mathbf{H}_{eff} the effective field, with contributions due to exchange, anisotropy, Zeeman, and demagnetizing energies. The simulated magnetic material is a 0.5 nm thick Co film in a Pt/Co/Pt multilayer with PMA. Micromagnetic parameters for the material are exchange stiffness

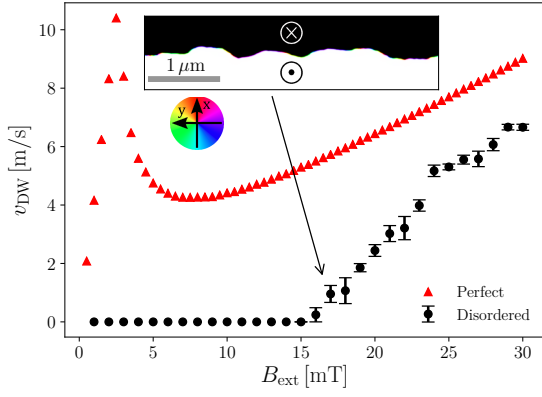


FIG. 1. v_{DW} as a function of B_{ext} in a perfect strip and in a disordered system where the disorder strength r has been tuned to roughly match the $v_{\text{DW}}(B_{\text{ext}})$ curve with the experimental one of Ref. [19]; the disorder-induced depinning field exceeds the Walker field of the perfect strip. Inset shows an example snapshot of a rough DW containing BLs in the disordered system with $B_{\text{ext}} = 17$ mT.

$A_{\text{ex}} = 1.4 \times 10^{-11}$ J/m, saturation magnetization $M_S = 9.1 \times 10^5$ A/m, uniaxial anisotropy $K_u = 8.4 \times 10^5$ J/m³ and damping parameter $\alpha = 0.27$; these have been experimentally determined in Ref. [19]. The resulting DW width parameter is $\Delta_{\text{DW}} = \sqrt{A_{\text{ex}}/K_0} \approx 7$ nm, where $K_0 = K_u - \frac{1}{2}\mu_0 M_S^2$ is the effective anisotropy. The system size is fixed to $L_x = 1024$ nm, $L_y = 4096$ nm and $L_z = 0.5$ nm. The simulation cell dimensions are $\Delta_x = \Delta_y = 2$ nm and $\Delta_z = 0.5$ nm. In every simulation the DW, separating domains oriented along $\pm z$, is initialized along the $+y$ direction as a Bloch wall with the DW magnetization in the $+y$ direction. Periodic boundary conditions are used in the y -direction to avoid boundary effects. The LLG equation is then solved using the Dormand-Prince solver (RK45) with an adaptive time step.

For thin films with thicknesses of only a few atoms, a natural source of disorder [25] is given by thickness fluctuations of the film. Thus, for simulations of disordered films, the sample is divided into “grains” of linear size 20 nm (defining the disorder correlation length) by Voronoi tessellation, each grain having a normally distributed random thickness $t_G = h + \mathcal{N}(0, 1)rh$, with r the relative magnitude of the grain-to-grain thickness variations, and h the mean thickness of the sample. These thickness fluctuations are then modeled using an approach proposed in Ref. [26], by modulating the saturation magnetization and anisotropy constant according to $M_S^G = \frac{M_S t_G}{h}$ and $K_u^G = \frac{K_u h}{t_G}$.

We start by considering the response of a Bloch DW to a constant B_{ext} along the $+z$ direction; this leads to DW motion in the $+x$ direction. Our algorithm solves the spatially averaged DW velocity v_{DW} by determining the local DW position along the DW as $X(y) = \min_y |m_z(x)|$,

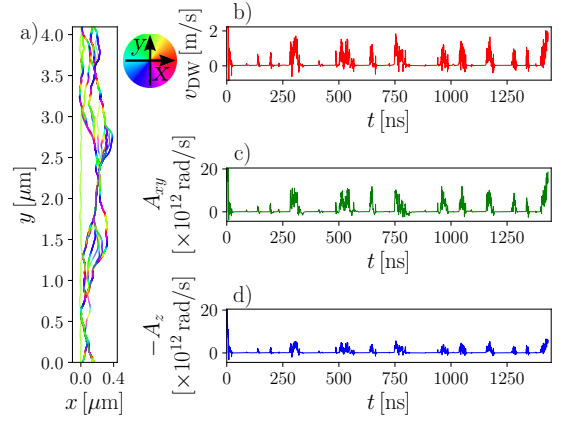


FIG. 2. a) An example of a sequence of DW magnetization configurations in between successive avalanches (as defined by thresholding the v_{DW} signal); the DW is moving to the $+x$ direction. The corresponding crackling noise signals, with b) the DW velocity $v_{\text{DW}}(t)$, c) the in-plane activity $A_{xy}(t)$, and d) the out-of-plane activity $-A_z(t)$.

with $m_z(x)$ interpolated across the minimum. By scanning different values of the thickness fluctuations r , we found that $r = 0.03$ produces a similar $v_{\text{DW}}(B_{\text{ext}})$ behavior as in the finite temperature experiments of Ref. [19] for the 0.5 nm thick sample in the range of 0 – 30 mT. Due to thermal rounding of the depinning transition [27] in experiments of Ref. [19] this value of r should be interpreted as a lower limit. The resulting $v_{\text{DW}}(B_{\text{ext}})$ curve is shown in Fig. 1, along with the corresponding curve from the disorder-free system. The depinning field of roughly 15 mT due to the quenched pinning field exceeds the Walker threshold of 2.5 mT of the non-disordered system, thus suggesting that the experiment of Ref. [19] is operating in the precessional regime.

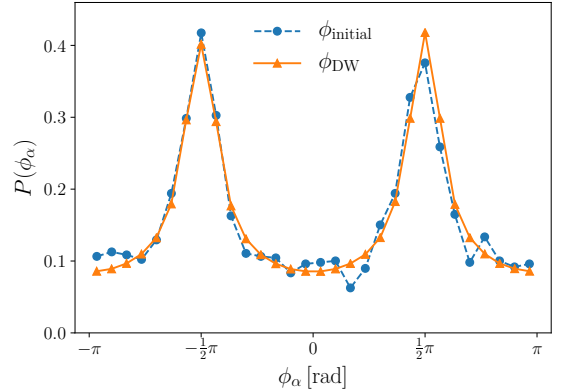


FIG. 3. Distribution of the in-plane magnetization angle ϕ_{initial} of the DW segments where avalanches are initiated, vs the corresponding distribution of ϕ_{DW} for all DW segments. The two distributions look almost identical, suggesting that the presence or absence of BLs within the DW is not important for the avalanche triggering process.

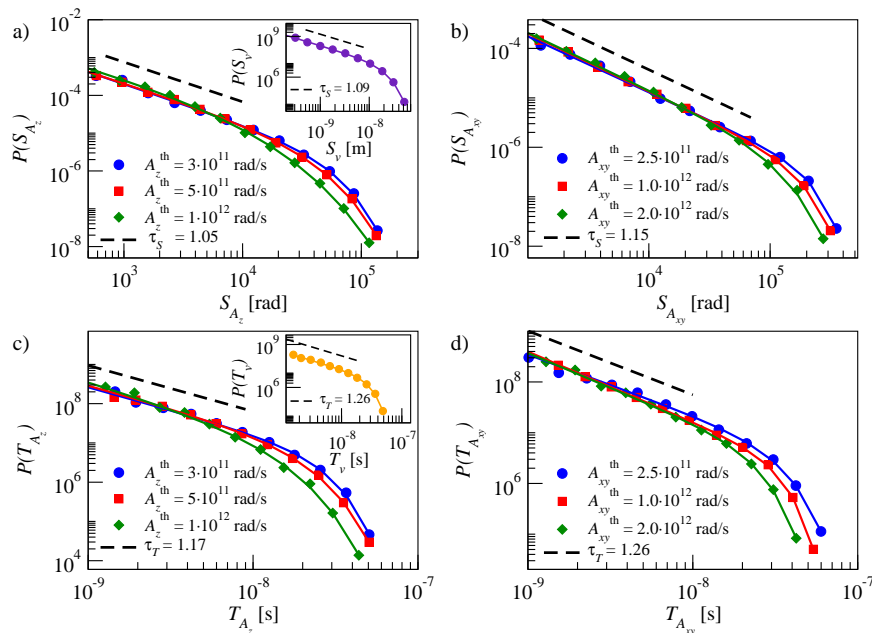


FIG. 4. Distributions of the avalanche sizes obtained by thresholding a) the $A_z(t)$ signal and b) the $A_{xy}(t)$ signal. The corresponding avalanche duration distributions are shown in c) and d), respectively. Different threshold values (A_z^{th} and A_{xy}^{th} , respectively) considered are indicated in the legends. The insets in a) and c) show the corresponding avalanche size and duration distributions computed from the $v_{\text{DW}}(t)$ signal using $v_{\text{DW}}^{\text{th}} = 0.1$ m/s. Solid lines correspond to fits of power-laws terminated by a large-avalanche cutoff (see text), while the dashed lines show the fitted power-law exponent in each case.

We then proceed to address the main problem of this paper, i.e., how Barkhausen noise is affected by the presence of BLs. To this end, we consider the system with $r = 0.03$, and a simulation protocol involving a moving simulation window where the DW center of mass is always kept within one discretization cell from the center of the simulation window, using the `ext_centerWall` function of MuMax3 with a modified tolerance. This minimizes effects due to demagnetizing fields that may slow down the DW during avalanches. To “re-introduce” this feature in a controllable fashion, we utilize a driving protocol analogous to the quasistatic limit of the constant velocity drive, where the driving field B_{ext} is decreased during avalanches (i.e., when $v_{\text{DW}} > v_{\text{DW}}^{\text{th}} = 0.1$ m/s) as $\dot{B}_{\text{ext}} = -k|v_{\text{DW}}|$, with $k = 0.18$ mT/nm chosen to adjust the avalanche cutoff to be such that the lateral extent of the largest avalanches is smaller than L_y , in order to avoid finite size effects. In between avalanches (i.e., when $v_{\text{DW}} < 0.1$ m/s), B_{ext} is ramped up at a rate $\dot{B}_{\text{ext}} = 0.037$ mT/ns until the next avalanche is triggered. The latter rate is chosen to get well-separated avalanches in time, while at the same time avoiding excessively long waiting times between avalanches. This leads to a $B_{\text{ext}}(t)$ which after an initial transient fluctuates in the vicinity of the depinning field.

To characterize the bursty DW dynamics, in addition to the “standard” DW velocity v_{DW} , we study different measures of the rate of spin rotation (or “activity”) associated with the DW dynamics. To study the dynamics of

the internal degrees of freedom of the DW, we consider separately contributions from in-plane and out-of-plane spin rotation, defined as $A_{xy}(t) = \sum_{i \in B} \dot{\phi}_i \cdot |\mathbf{m}_{i,xy}|$ and $A_z(t) = \sum_{i \in B} \dot{\theta}_i$, respectively, where ϕ_i and θ_i are the spherical coordinate angles of the magnetization vector \mathbf{m}_i in the i th discretization cell. The sums are taken over a band B extending 20 discretization cells around the DW on both sides, moving with the DW. The multiplication by $|\mathbf{m}_{i,xy}|$ in A_{xy} is included to consider only contributions originating from inside of the DW.

Fig. 2a) shows examples of DW magnetization configurations in between successive avalanches, defined by thresholding the $v_{\text{DW}}(t)$ signal with $v_{\text{DW}}^{\text{th}} = 0.1$ m/s. To quickly reach the stationary avalanche regime, we use 15 mT as the initial field. Notice how the initially straight Bloch DW (green) is quickly transformed into a rough interface with a large number of BLs, visible in Fig. 2a) as abrupt changes of color along the DW; see also Movie 1 (Supplementary Material [28]).

Figs. 2b), c) and d) show the corresponding $v_{\text{DW}}(t)$, $A_{xy}(t)$ and $-A_z(t)$ signals, respectively; notice that $A_z(t)$ has a minus sign to compensate for the fact that B_{ext} along $+z$ tends to decrease θ_i . In addition to the fact that all three signals exhibit the characteristic bursty appearance of a crackling noise signal, we observe two main points: (i) v_{DW} , as well as the two activity signals $A_{xy}(t)$ and $-A_z(t)$, may momentarily have negative values; this indicates that the DW center of mass

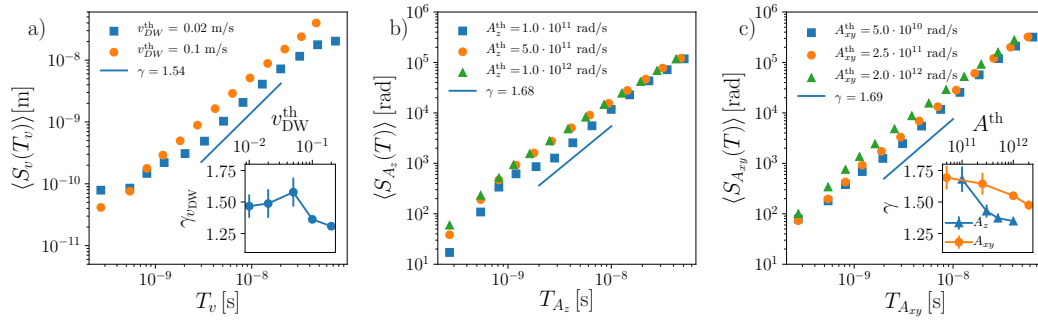


FIG. 5. Scaling of the average avalanche size as a function of duration for different threshold values. a) $\langle S_v(T_v) \rangle$, b) $\langle S_{A_z}(T) \rangle$ and c) $\langle S_{A_{xy}}(T) \rangle$. The insets in a) and c) illustrate the threshold-dependent nature of the exponent γ characterizing the size vs duration scaling.

is moving against the direction imposed by B_{ext} , and hence the DW does not respect the Middleton theorem [22]. (ii) While the appearance of the three signals is quite similar, $A_{xy}(t)$ has a significantly larger magnitude than $A_z(t)$: We find $\langle A_{xy}/A_z \rangle \approx 1.7$, showing that in relative terms the BL activity within the DW is more pronounced during avalanches than the overall propagation of the DW. Comparing the distribution $P(\phi_{\text{initial}})$ of the local in-plane magnetization angle ϕ_{initial} of the DW segments from which an avalanche is triggered to that of the angle ϕ_{DW} of all DW segments (Fig. 3) suggests that the avalanche triggering process is not affected by the local DW structure.

To analyze the statistical properties of the Barkhausen avalanches, we consider 200 realizations of the three signals discussed above. Denoting the signal by $V(t)$, the avalanche size is defined as $S_V = \int_0^T [V(t) - V^{\text{th}}] dt$, where V^{th} is the threshold level used to define the avalanches; the integral is over a time interval T (the avalanche duration) during which the signal stays continuously above V^{th} . We consider separately the three cases where $V(t)$ is $v_{\text{DW}}(t)$, $A_z(t)$ or $A_{xy}(t)$. Figs. 4 a) and b) show the distributions $P(S_{A_z})$ and $P(S_{A_{xy}})$ for different threshold values (A_z^{th} and A_{xy}^{th} , respectively); The corresponding avalanche duration distributions $P(T_{A_z})$ and $P(T_{A_{xy}})$ are shown in Figs. 4 c) and d), respectively. Insets of Figs. 4 a) and c) show the distributions $P(S_v)$ and $P(T_v)$ extracted from the v_{DW} signal using $v_{\text{DW}}^{\text{th}} = 0.1$ m/s.

All the distributions can be well-described by a power law terminated by a large-avalanche cutoff. Solid lines in Fig 4 show fits of $P(S_V) = S_V^{-\tau_S} \exp[-(S_V/S_V^*)^\beta]$, where τ_S is a scaling exponent, β parametrizes the shape of the cutoff, and S_V^* a cutoff avalanche size (avalanche durations follow a similar scaling form). We find $\tau_S = 1.1 \pm 0.1$ and $\tau_T = 1.2 \pm 0.1$, respectively, i.e. close to the values expected for the quenched Edwards Wilkinson (qEW) equation, $\partial h(x, t)/\partial t = \nu \nabla^2 h(x, t) + \eta(x, h) + F_{\text{ext}}$, describing a short-range elastic string $h(x, t)$ driven by an external force F_{ext} in a quenched random medium η [29]. The value of the τ_S exponent is also close to that found

very recently for “creep avalanches” [30], and to that describing avalanches in the central hysteresis loop in a 2D RFIM with a built-in DW [31]. The cutoff avalanche size and duration depend on the imposed threshold level, but appear to saturate to a value set by the “demagnetizing factor” k in the limit of a low threshold. Fig. 5 shows the scaling of the average avalanche size as a function of duration, $\langle S_v(T) \rangle$ in a), $\langle S_{A_z}(T) \rangle$ in b) and $\langle S_{A_{xy}}(T) \rangle$ in c). The exponent γ describing the scaling as $\langle S_v(T) \rangle \sim T^\gamma$ (and similarly for $\langle S_{A_z}(T) \rangle$ and $\langle S_{A_{xy}}(T) \rangle$) is found to be threshold-dependent, in analogy to recent observations for propagating crack lines [32] and the RFIM [33], with the γ -value close to 1.6 expected for the qEW equation in the limit of zero threshold [2] approximately recovered for low thresholds [insets of Fig. 5a) and c)]. Thus, our exponent values satisfy within error bars the scaling relation $\gamma = (\tau_T - 1)/(\tau_S - 1)$.

Hence, we have shown how DWs with a dynamical internal structure consisting of BLs generate Barkhausen noise in disordered thin films with PMA. One of the unique features of this system is the large relative magnitude of the internal, in-plane bursty spin rotation activity within the DW, which in our case actually exceeds that of the out-of-plane spin rotations contributing to DW displacement. We have demonstrated that this internal dynamics within the DW leads to a violation of the Middleton “no-passing” theorem.

It is quite remarkable that the scaling exponents describing the Barkhausen jumps cannot be distinguished from those expected for the much simpler qEW equation. The avalanche triggerings appear not to be correlated with the internal structure of the DW. Thus, commonly used simple models based on describing DWs as elastic interfaces, neglecting Bloch line dynamics by construction, seem to be capturing correctly the large-scale critical dynamics of the system. This may be rationalized by noticing that Bloch lines, being localized Néel wall -like segments within the Bloch DW, produce dipolar stray fields decaying as $1/r^3$ in real space. For $1d$ interfaces, such interactions are short-ranged, and hence

are not expected to change the universality class of the avalanche dynamics from that of systems with purely local elasticity. In higher dimensions dipolar interactions are long-ranged, so we expect that the internal dynamics of the DWs will have important consequences; the role of Bloch lines in the case of $3d$ magnets with $2d$ DWs should be addressed in future studies. Another important future avenue of research of great current interest would be to extend the present study to thin films with Dzyaloshinskii-Moriya interactions [34, 35].

This work has been supported by the Academy of Finland through an Academy Research Fellowship (LL, project no. 268302). We acknowledge the computational resources provided by the Aalto University School of Science “Science-IT” project, as well as those provided by CSC (Finland).

* lasse.laurson@tuni.fi

- [1] G. Durin and S. Zapperi, in *The Science of Hysteresis*, edited by G. Bertotti and I. Mayergoyz (Academic, Amsterdam, 2006).
- [2] L. Laurson, X. Illa, S. Santucci, K. T. Tallakstad, K. J. Måløy, and M. J. Alava, *Nat. commun.* **4**, 2927 (2013).
- [3] M. Rost, L. Laurson, M. Dubé, and M. Alava, *Phys. Rev. Lett.* **98**, 054502 (2007).
- [4] S. Zapperi, P. Cizeau, G. Durin, and H. E. Stanley, *Phys. Rev. B* **58**, 6353 (1998).
- [5] H. Barkhausen, *Phys. Z* **20**, 401 (1919).
- [6] V. Lecomte, S. E. Barnes, J.-P. Eckmann, and T. Giamarchi, *Phys. Rev. B* **80**, 054413 (2009).
- [7] S. S. Parkin, M. Hayashi, and L. Thomas, *Science* **320**, 190 (2008).
- [8] N. L. Schryer and L. R. Walker, *J. Appl. Phys.* **45**, 5406 (1974).
- [9] A. Mougin, M. Cormier, J. Adam, P. Metaxas, and J. Ferré, *EPL* **78**, 57007 (2007).
- [10] A. Thiaville and Y. Nakatani, in *Spin dynamics in confined magnetic structures III* (Springer, 2006) pp. 161–205.
- [11] T. Herranen and L. Laurson, *Phys. Rev. B* **92**, 100405 (2015).
- [12] T. Herranen and L. Laurson, *Phys. Rev. B* **96**, 144422 (2017).
- [13] A. Malozemoff and J. Slonczewski, *Magnetic Domain Walls in Bubble Materials* (Academic press, 1979).
- [14] L. Laurson, G. Durin, and S. Zapperi, *Phys. Rev. B* **89**, 104402 (2014).
- [15] N. B. Caballero, E. E. Ferrero, A. B. Kolton, J. Curiale, V. Jeudy, and S. Bustingorry, *Physical Review E* **97**, 062122 (2018).
- [16] F. J. Pérez-Reche and E. Vives, *Physical Review B* **70**, 214422 (2004).
- [17] A. Mughal, L. Laurson, G. Durin, and S. Zapperi, *IEEE Trans. Magn.* **46**, 228 (2010).
- [18] D. Spasojević, S. Janičević, and M. Knežević, *Physical Review E* **84**, 051119 (2011).
- [19] P. Metaxas, J. Jamet, A. Mougin, M. Cormier, J. Ferré, V. Baltz, B. Rodmacq, B. Dieny, and R. Stamps, *Phys. Rev. Lett.* **99**, 217208 (2007).
- [20] D.-H. Kim, S.-B. Choe, and S.-C. Shin, *Phys. Rev. Lett.* **90**, 087203 (2003).
- [21] S. Papanikolaou, F. Bohn, R. L. Sommer, G. Durin, S. Zapperi, and J. P. Sethna, *Nat. Phys.* **7**, 316 (2011).
- [22] A. A. Middleton, *Phys. Rev. Lett.* **68**, 670 (1992).
- [23] P. Le Doussal, K. J. Wiese, and P. Chauve, *Phys. Rev. B* **66**, 174201 (2002).
- [24] A. Vansteenkiste, J. Leliaert, M. Dvornik, M. Helsen, F. Garcia-Sanchez, and B. Van Waeyenberge, *AIP advances* **4**, 107133 (2014).
- [25] J. Leliaert, B. Van de Wiele, A. Vansteenkiste, L. Laurson, G. Durin, L. Dupré, and B. Van Waeyenberge, *Journal of Applied Physics* **115**, 17D102 (2014).
- [26] S. Moretti, M. Voto, and E. Martinez, *Phys. Rev. B* **96**, 054433 (2017).
- [27] S. Bustingorry, A. Kolton, and T. Giamarchi, *EPL* **81**, 26005 (2007).
- [28] See Supplemental Material at [URL will be inserted by the publisher] for a movie illustrating the bursty dynamics of a DW containing Bloch lines.
- [29] A. Rosso, P. Le Doussal, and K. J. Wiese, *Phys. Rev. B* **80**, 144204 (2009).
- [30] M. P. Grassi, A. B. Kolton, V. Jeudy, A. Mougin, S. Bustingorry, and J. Curiale, *arXiv preprint arXiv:1804.09572* (2018).
- [31] B. Tadić, *Physica A: Statistical Mechanics and its Applications* **493**, 330 (2018).
- [32] S. Janičević, L. Laurson, K. J. Måløy, S. Santucci, and M. J. Alava, *Phys. Rev. Lett.* **117**, 230601 (2016).
- [33] S. Janičević, D. Jovković, L. Laurson, and D. Spasojević, *Sci. Rep.* **8**, 2571 (2018).
- [34] A. Thiaville, S. Rohart, É. Jué, V. Cros, and A. Fert, *EPL* **100**, 57002 (2012).
- [35] Y. Yoshimura, K.-J. Kim, T. Taniguchi, T. Tono, K. Ueda, R. Hiramatsu, T. Moriyama, K. Yamada, Y. Nakatani, and T. Ono, *Nat. Phys.* **12**, 157 (2016).